RSC Advances

PAPER

View Article Online
View Journal | View Issue

Cite this: *RSC Adv.*, 2019, **9**, 17698

A novel ultrasensitive surface plasmon resonance-based nanosensor for nitrite detection†

Pandeng Miao,[ab] Zhongdong Liu,*[a] Jun Guo,[b] Ming Yuan,[b] Ruibo Zhong,[b] Liping Wang *[c] and Feng Zhang *[bc]

Received 1st April 2019
Accepted 21st May 2019

DOI: 10.1039/c9ra02460c

rsc.li/rsc-advances

Nitrite is a common food additive, however, its reduction product, nitrosamine, is a strong carcinogen, and hence the ultra-sensitive detection of nitrite is an effective means to prevent related cancers. In this study, different sized gold nanoparticles (AuNPs) were modified with *P*-aminothiophenol (ATP) and naphthylethylenediamine (NED). In the presence of nitrite, satellite-like AuNPs aggregates formed *via* the diazotization coupling reaction and the color of the system was changed by the functionalized AuNPs aggregates. The carcinogenic nitrite content could be detected by colorimetry according to the change in the system color. The linear concentration range of sodium nitrite was 0–1.0 μg mL^{-1} and the detection limit was determined to be 3.0 ng mL^{-1}. Compared with the traditional method, this method has the advantages of high sensitivity, low detection limit, good selectivity and can significantly lower the naked-eye detection limit to 3.0 ng mL^{-1}. In addition, this method is suitable for the determination of nitrite in various foods. We think this novel designed highly sensitive nitrate nanosensor holds great market potential.

1. Introduction

Cancer is a symptom of normal somatic cells mutating into infinitely increasing cancer cells and is one of the main diseases threatening public health and lives at present.[1] The high mortality rate of cancer is mainly due to the fact that cancer is difficult to detect, especially in the early stage considered as the best window-period for treatment, and cancer prevention is the most effective means to defeat it at this stage.[2] However, at present, it is confirmed usually in the middle or late stages of cancer, leading to irreparable damage. Due to the unique physicochemical properties of nanomaterials, nanosensors show great potential in biomedical applications, and the surface plasmon resonance of AuNPs has been widely used in colorimetric detection.

Nitrite is a very common food additive,[3] added into sausages, jams, meat emulsions and other foods at different dosages, mainly as colouring agents and preservatives. Nitrite inhibits many harmful microorganisms, especially clostridium botulinum. Nitrite can be used as an antioxidant to reduce food oxidation caused by light, heat, oxygen, microorganisms and other factors during processing and storage and it can reduce the harmful flavour and toxic substances produced in the process of oxidation. However, in recent years, the illegal addition of nitrite in foods and its high carcinogenicity has been exposed more and more, and the high carcinogenicity of nitrite[4–6] has made us recognize the necessity and urgency of ultra-sensitive detection of nitrite.[7,8] Nitrite is a highly toxic substance; its adult poisoning dose is 0.2–0.5 g and the lethal dose is 3.0 g. Under stomach acid conditions, nitrite can react with secondary amines, tertiary amines and amides in foods to form the strong carcinogen *N*-nitrosamine. Normal oxygen-carrying haemoglobin in blood can be oxidized to methaemoglobin by nitrite, losing the oxygen carrying capacity and causing hypoxia.[9] In addition, nitrosamines can enter a foetus through the placenta, which has a stagnating effect on the foetus development; infants under 6 months of age are particularly sensitive to nitrite. Clinical symptoms of methaemoglobin in children are caused by eating foods with high concentrations of nitrite and the resulting symptoms are hypoxia, purpura, or even death.[10]

The nitrite detection methods at present mainly include spectroscopy,[11–14] chromatography[15–19] and electrochemical methods.[20–23] The spectroscopic methods include ultraviolet-visible (UV-vis) spectrophotometry, phenol spectrophotometry, flow injection spectrophotometry, and coefficient compensation dual wavelength spectrophotometry; the current detection range of nitrite is 0–1.2 g mL^{-1} and the

[a]*Grain College, Henan University of Technology, Zhengzhou 450001, P. R. China. E-mail: liuzhongdong@aliyun.com*

[b]*State Key Laboratory of Respiratory Disease, Key Laboratory of Oral Medicine, Guangzhou Institute of Oral Disease, Stomatology Hospital, Department of Biomedical Engineering, School of Basic Medical Sciences, Guangzhou Medical University, Guangzhou 511436, P. R. China. E-mail: fengzhang1978@hotmail.com*

[c]*School of Biomedical Engineering, Shanghai Jiaotong University, Shanghai 200241, P. R. China. E-mail: lpingwang@sjtu.edu.cn*

† Electronic supplementary information (ESI) available: Traditional methods for detecting nitrite (colorimetric method) and the TEM images of the AuNPs. See DOI: 10.1039/c9ra02460c

detection limit is 0.01 μg mL^{-1}.[11–14] Chromatography methods mainly include high performance liquid chromatography (HPLC), ion chromatography (IC) and gas chromatography (GC) with detection limits of 0.025 μg mL^{-1}, 0.015 μg mL^{-1} and 0.609 mg kg^{-1}, respectively. The electrochemical methods include polarography, nitrate electrode method and capillary electrophoresis with a detection limit of 0.8 μg mL^{-1}.[20–23] Sakthinathan *et al.* prepared a novel and selective nitrite sensor based on the non-covalent interactions of a Schiff base copper complex, using a RGO/[Cu(sal-ala)(phen)] modified glass carbon electrode to determine the nitrite content, and the detection limit reached 19 nM.[24] With the development of nanotechnology, nanoparticles were used to modify the electrode. Tamizhdurai *et al.* synthesized CeO_2 nanoparticles by an environmentally friendly method and used modified glassy carbon electrode (GCE) with CeO_2 NPs for the detection of nitrite with a low limit of detection (0.21 μM).[25] Weston *et al.* developed novel sulfanilamide and naphthylethylenediamine functionalized AuNPs with nitrite-reactive groups that take advantage of their optical properties and can be used to colorimetrically detect nitrite or nitrate ions at a nitrite concentration between 22 and 30 μM.[26] In addition, citric acid, *p*-aminobenzenesulfonamide and *N*-(1-naphthyl)ethylenediamine hydrochloride have been used as chromogenic agents in a rapid nitrite detection paper-chip device with colorimetric detection; the detection limit was 5 μg mL^{-1}.[27]

In our lab, we found that the chromogenic reaction of ATP modified AuNPs with nitrite and NED was much more obvious than with ATP alone. Therefore, in this study, we designed satellite-like nanostructures, in which different-sized AuNPs were respectively modified with ATP and NED.[28] In the presence of nitrite, numerous smaller AuNPs were conjugated to the larger AuNPs and formed satellite-like aggregates *via* a diazotization coupling reaction. The colour change showed a linear correlation to the nitrite concentration and the naked-eye detection limit reduced to 5 ng mL^{-1}, which is much lower than the international safety standard limit of nitrite (4 μg mL^{-1}).[29–31]

2. Experimental section

2.1. Chemicals and equipment

Hydrated chloroauric acid ($HAuCl_4 \cdot 4H_2O$) was purchased from Alfa Aesar. ATP, NED, 1-ethyl-3-(3-dimethylaminopropyl) carbodiimide (EDC), and sodium citrate were purchased from Tokyo Chemical Industry (TCI). Potassium ferrocyanide and zinc acetate were purchased from Macklin. Absolute ethanol was purchased from Sinopharm Chemical Reagent Co., Ltd (SCRC). All reagents were used directly without further purification. The food materials used in the experiments were purchased randomly. Both UV-vis spectrophotometer (U-2900, Hitachi) and multi-function microplate reader (Super Max-3100, Shanghai Flash) were used for absorbance measurements and monitoring. The hydrodynamic size and ζ potential

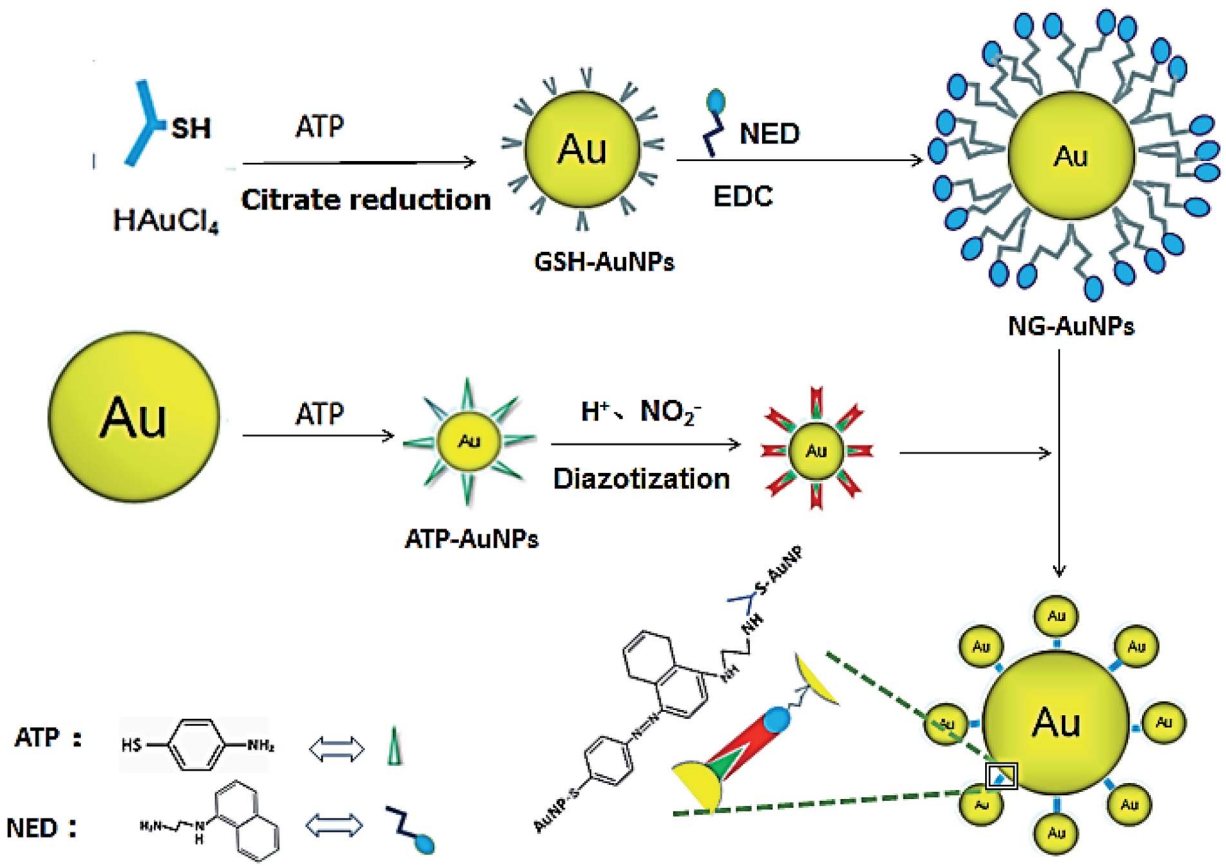

Fig. 1 The schematic of NO_2^- detection by Au satellite-like aggregate colorimetry.

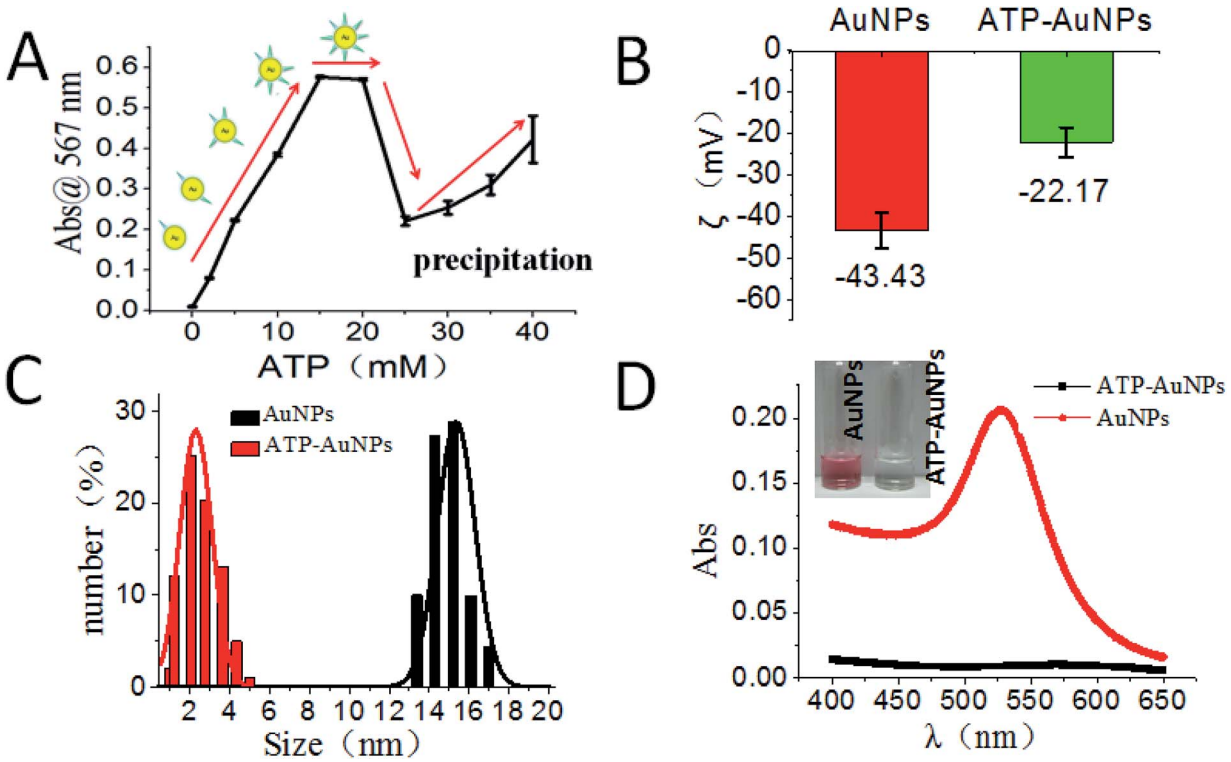

Fig. 2 Characterization of ATP-AuNPs. (A) The absorption was monitored at 567 nm for citrate-protected AuNPs etched by ATP at different concentrations. The inset cartoons represent the changing of ATP ligand numbers capped on AuNPs. (B) The zeta potential (ζ) change before and after ATP conjugation to AuNPs. (C) The hydrodynamic size change before and after ATP conjugation to AuNPs. (D) UV absorption and colour change (inset) before and after ATP conjugation to AuNPs.

were determined by a dynamic light scattering (DLS) equipment (Zetasizer, ZS90, Malvern).

2.2. AuNPs preparation

Sodium citrate reduction method: 17 mg of $HAuCl_4 \cdot 4H_2O$ was dissolved in 50 mL deionized water; then the solution was refluxed for 10 min and the colour became pale yellow. 78 mg of sodium citrate was dissolved in 5 mL of deionized water; the sodium citrate solution was pre-warmed to 60–70 °C and was then quickly added to the hydrated chloroauric acid solution. The mixture was refluxed for 20 min and its colour changed from yellow to colourless, gradually deepening to bright dark red. The reacted solution was cooled to room temperature (RT), the pH value of the solution was adjusted to 7.0, the solution was filtered twice by 0.45 μm membrane filter, and the collected AuNPs were kept at RT for later use. The average size of the obtained AuNPs is about 17.0 nm and the concentration was determined to be about 10^{-8} M by the Beer–Lambert law.

10 mL of glutathione (GSH, 0.01 M) was added to 10 mL $HAuCl_4$ solution (0.01 M) and stirred for 30 min; then, the mixture was added into 1 mL sodium borohydride (0.1 M) solution and stirred for another 2 h. The mixture was filtered twice by 0.45 μm membrane filter and the collected AuNPs were kept at RT for later use. The average size of GSH modified AuNPs (G-AuNPs) was ~10.0 nm and the concentration was determined to be 10^{-7} M by the Bouguer–Lambert–Beer law: $A = \varepsilon \times c \times l$,[32,33] where A is the absorbance value, ε is the extinction coefficient and l is the path length of the light passing through the sample (cm). For AuNPs with 10 nm diameter, $\varepsilon_{520\ nm} = 1.37 \times 10^8\ M^{-1}\ cm^{-1}$.

2.3. The functionalization of AuNPs

Modification of ATP: (i) 15 nm AuNP solution was mixed with 15 mM ATP in ethanol solution at a volume ratio of 9 : 1; the pH value of the mixture was adjusted to 3.0, and it was stirred for 3 h at 70 °C. The solution colour changed from pink to colourless and the resulting AuNPs were labelled as ATP-AuNPs. During this process, the colour, particle size and surface potential of AuNPs varied significantly. (ii) 10 mL of G-AuNPs were thoroughly mixed with 10 mL NED (20 mM) in sodium borate buffer (50 mM, pH 9.0, hereafter abbreviated as SB9) and 10 mL of EDC (1.0 M) and reacted at RT for 2 h. After reacting, the AuNPs were purified using ultrafiltration filters. NED concentration conjugated to G-AuNPs was determined to be 0.21 mM and the resulting AuNPs were labelled as NG-AuNPs.

2.4. Preparation of sodium nitrite standard solution

Accurately weighed 10 mg sodium nitrite was dissolved in 50 mL deionized water; the concentration of this solution was 200 μg mL^{-1} and was used as sodium nitrite mother liquor. The solution was diluted to prepare 0.005, 0.01, 0.05, 0.1, 0.2, 0.5, 1.0, 3.0, 5.0, 10, 15, 20 and 25 μg mL^{-1} standard solutions.

2.5. Preparation of food extracted sample solutions

0.25 g samples taken from bread, milk, pork luncheon meat, ham, and spicy cabbage were crushed into pulp and then soaked in a 25 mL aqueous solution with 30 min sonication. After centrifugation, 5 mL of the supernatant was taken and mixed with 200 μL of potassium ferrocyanide solution (10^6 g L^{-1}) and 0.5 mL of zinc acetate solution (220 g L^{-1}) with vigorous stirring for 5–10 min. Finally, the extracted aqueous samples were obtained by filtration and stored in a refrigerator at −4 °C for later detection. The original nitrite concentrations of these samples were calculated by multiplying by 100.

3. Results and discussion

Our reaction scheme (Fig. 1) was designed as follows: the diazotization reaction happens between ATP-AuNPs and NO_2^- under acidic conditions; then ATP-AuNPs react with NG-AuNPs by a coupling reaction and the colour of the reaction solution obviously changes. The maximum absorption peak of the solution was at 567 nm and the absorption value was positively correlated to the concentration of NO_2^- within a certain range.

In order to select the optimum concentration of ATP connected to AuNPs, the UV adsorption of AuNPs at 567 nm was

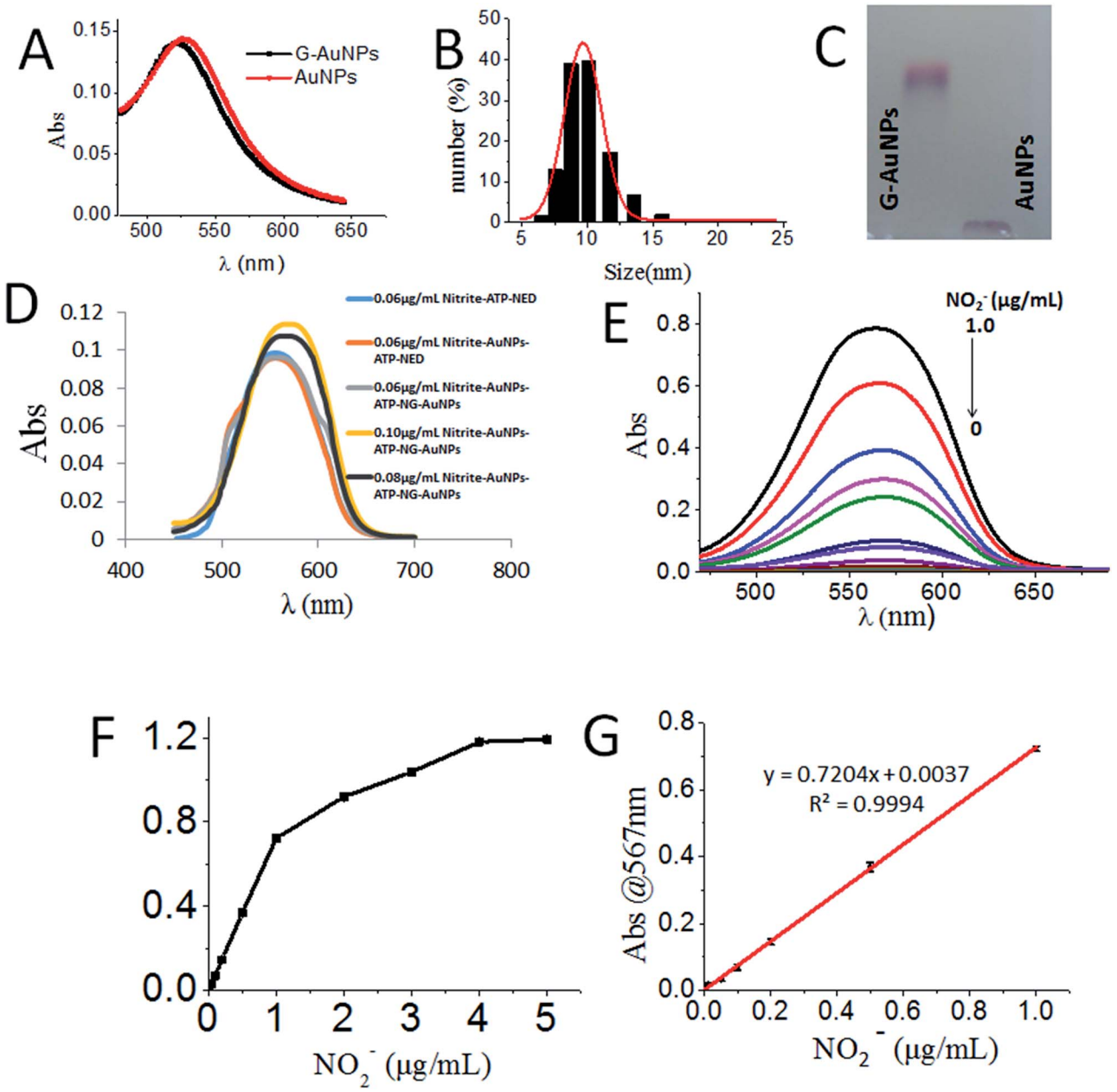

Fig. 3 Characterization, covalent conjugation and nitrite detection of NG-AuNPs. (A) UV-vis absorption spectrum of G-AuNP. (B) Size distribution of G-AuNPs measured by DLS. (C) Agarose gel electrophoresis of G-AuNPs and citrate-protected AuNPs. (D) Brief description of the detection principle of the system. (E) Absorption spectra of NO_2^- with gradient concentrations in the system. (F) The raw 567 nm-absorbance plot in a larger concentration range. (G) Plot of 567 nm-absorbance with a linear fit (red line) function ($y = 0.7204x + 0.0037$, where y is the 567 nm-absorbance and x is the concentration of NO_2^-).

monitored with different concentrations of ATP added into the AuNP solutions with the same amounts of hydrochloric acid, nitrite, and NED in the system. When the ATP concentration was below 15 mM, the absorbance value of the system rose along with the increase in the ATP concentration. When ATP concentration increased to 15–20 mM, the adsorption remained the same. When the ATP concentration was above 20 mM, the increase in the ATP concentration caused the system to become unstable; aggregation and precipitation began to occur, resulting in a sharp decrease in the absorption. Due to the aggregation and precipitation of the AuNPs, the standard error became large as the ATP concentration increased over 20 mM. The zeta potential, particle size and UV absorption changes before and after the reaction are shown in Fig. 2B, C and D, respectively. In the etching process of AuNPs by ATP, ATP was connected to AuNPs by the Au–S bond.[34,35] The zeta potential of ATP-AuNPs increased to −22.17 mV from −43.43 mV (AuNPs), which proved the formation of ATP-AuNPs. The particle size of ATP-AuNPs decreased greatly, to 2 nm from 15 nm (AuNPs), because of the etching effect. The adsorption of AuNPs is related to the size of the particle. At the same concentration, the smaller the particle size is, the weaker is the adsorption. When the gold particle size was 2 nm, almost no adsorption was observed. The ATP-AuNPs size decreased to 2 nm, and hence no adsorption was observed in the ATP-AuNPs solution.

The GSH-protected AuNPs (GSH-AuNPs) showed a typical surface plasmon peak at ~520 nm (Fig. 3A) and their average hydrodynamic size was about 10.0 nm as determined by DLS (Fig. 3B). By running AuNPs on agarose gel electrophoresis (AGE), we verified that GSH was covalently conjugated to AuNPs by Au–S bonds and the resulting GSH-AuNPs were more robust than citrate-protected AuNPs on AGE (Fig. 3C). The as-prepared GSH-AuNPs were further conjugated with NED to prepare NG-AuNPs. The free NED was removed by centrifugation and ultrafiltration. The final concentration of conjugated NED to GSH-AuNP was determined to be 2.52 μM and the concentration of NG-AuNP was 1.78 nM, so the final molar ratio of NED to GSH-AuNP was ~1.42×10^3, which indicated a very high covalent conjugation efficiency. We investigated the adsorption changes in the coloured chromophore formed in the system. As shown in Fig. 3D, when nitrite just reacted with ATP and NED, the adsorption spectrum of the formed chromophore was narrow. After AuNPs were modified by ATP, ATP-AuNPs reacted with NED and nitrite to form a coloured chromophore; the characteristic shoulder peak of AuNPs at 517 nm was also observed because the ATP-AuNPs were not aggregated. When low concentration nitrite reacted with NG-AuNPs and ATP-AuNPs, the formed AuNPs aggregation was co-excited with the unreacted NG-AuNPs and ATP-AuNPs in the system, so a wider peak was observed around 600–650 nm corresponding to the adsorption of AuNPs and AuNP aggregations. With the increase in the nitrite concentration, the characteristic peak of AuNPs weakened and the aggregation peak was more obvious; a relatively smooth peak was observed. The system is shown in Fig. 3E. The detection limit of NO_2^- was determined to be 3 ng mL^{-1} with a signal-to-noise ratio of 3. As shown in Fig. 3F and G, the plot of absorption at 567 nm against NO_2^- concentration showed a good linear correlation for NO_2^- concentrations ranging from 0 to 1.0 μg mL^{-1}.

The sensing system was further tested under different pH conditions and in the presence of different ions. The sensors showed colorimetric changes (distinguishable by naked eye) only under acidic conditions (*i.e.* from pH 1.0 to 6.0, Fig. 4A). The sensing system showed the highest selectivity for NO_2^- among different ions; though Fe^{2+}, Fe^{3+}, and Cu^{2+} also responded with slight colour changes, their absorption was more than 4-fold less sensitive compared to that of NO_2^- (Fig. 4B).

To apply the current sensor to real food samples, aqueous samples were extracted from different foods and tested for NO_2^-. The nitrite detection results were compared between the current nanosensor system and the traditional method based on *p*-aminobenzenesulfonic acid undergoing diazotization reaction with NO_2^- and naphthylethylenediamine under acidic conditions to form dye molecules where the colour depth is positively correlated with the concentration of NO_2^- (ESI†).

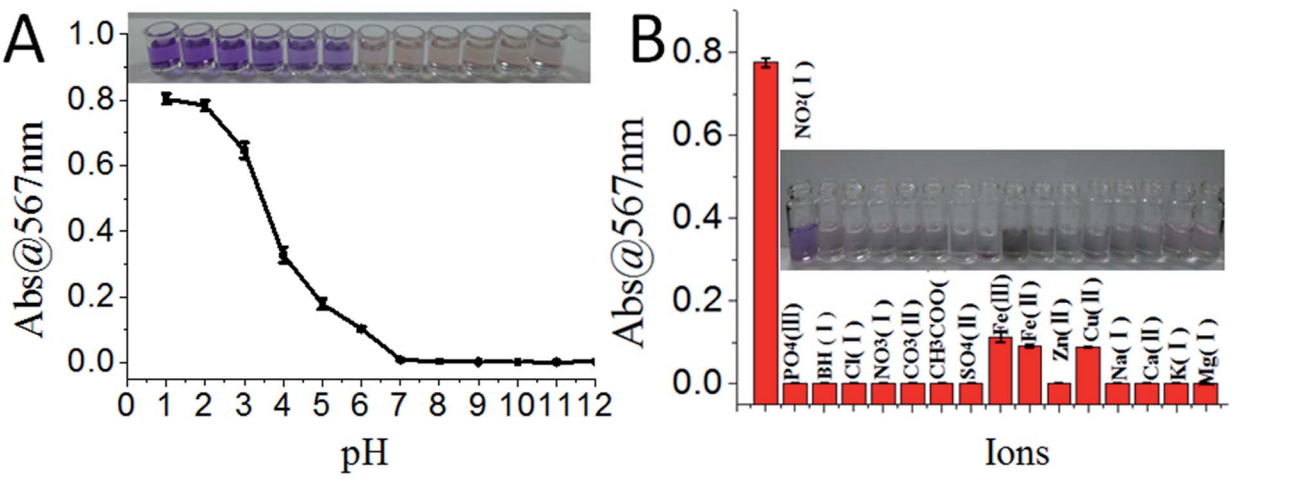

Fig. 4 The sensitivity and selectivity of the sensing system. (A) Colorimetric changes of the sensing system in the presence of NO_2^- (1.0 μg mL^{-1}) under different pH conditions. (B) The ionic selectivity test of the sensing system; inset is the absorbance at 567 nm monitored with the addition of equimolar ions.

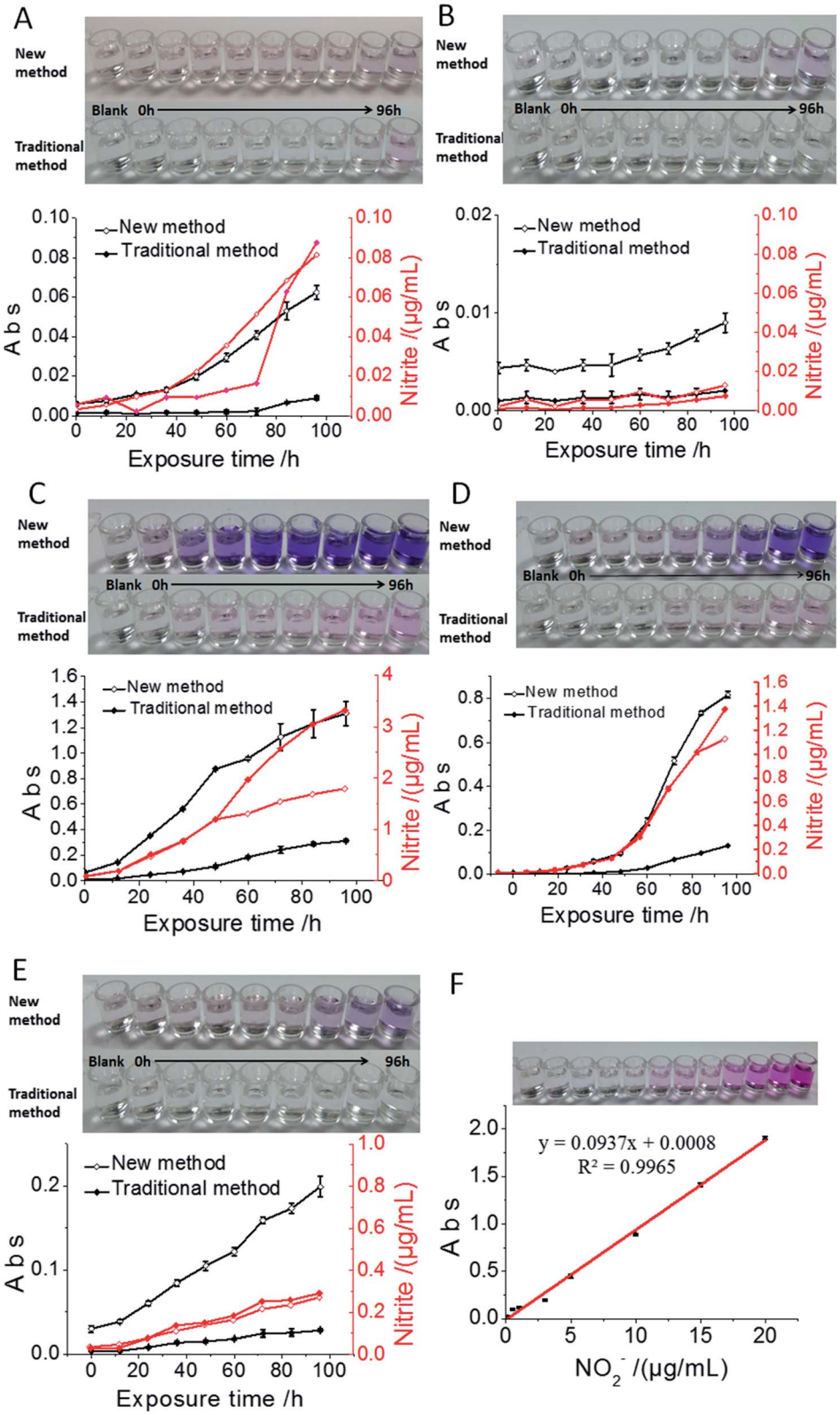

Fig. 5 Application of the nanosensor to nitrite detection for samples of bread (A), milk (B), pork luncheon meat (C), ham (D) and spicy cabbage (E). The photos are of the real tested samples and the plots below are 567 nm-absorbance against the food exposure time in a −4 °C refrigerator. The comparisons of chromogenic effects between the new method and traditional method are shown in both photos and plots. (F) The standard detection plot derived from the traditional detection method showed a detection limit of 0.06 g mL^{-1}.

China's allowable nitrite residues in bread, milk, pork luncheon meat, ham and spicy cabbage are 2 μg mL^{-1}, 0.2 μg mL^{-1}, 50 μg mL^{-1}, 70 μg mL^{-1} and 20 μg mL^{-1}, respectively. In the bread sample, because of the low nitrite content, the observable colour change started after 84 h exposure time using the traditional method, while it was reduced to 36 h using the current nanosensor (Fig. 5A). The nitrite content in milk was very low; after 60 h exposure in the air, the nitrite content in milk reached just 3 ng mL^{-1}, which could not be detected by the traditional method. However, there was obvious colour change by the new method, confirming the advantage of the low detection limit of the current nanosensor (Fig. 5B). The nitrite content in the pork luncheon meat was very high; the nitrite content of the sample reached a saturated state after 48 h exposure, which also showed higher sensitivity compared to the traditional method (Fig. 5C). As for the ham sample, we found that the nitrite content exceeded the allowable amount after 60 h exposure in air using both methods; however, the nanosensor showed apparent sensitivity advantages over the traditional method (Fig. 5D). In the pickling process for hot cabbage in factories, the cabbages are generally stored for more than 20 days. The lactic acid bacteria in the products can consume nitrite, so the nitrite content of samples increased slowly (Fig. 5E), but normally it is not suitable to store cabbage for more than 48 h. Through the detection of different food and drink samples, we found that the current nanosensor showed a lower detection limit compared with the traditional method, in which lower nitrite content in foods can be observed with just naked eye. For the current nanosensor, the optimum detection range was 0–1.0 ng mL^{-1} and the detection limit was 3.0 ng mL^{-1}. According to these detection results, we strongly suggest that the above-detected foods should be used up within 36 hours after unpacking, even if stored in the refrigerator, otherwise one risks having dangerous foods with nitrite levels exceeding the international standard.

4. Conclusion

The current research reported a novel nitrite detection method and built an applicable nanosensor with a significantly reduced detection limit compared to the traditional detection method. The nanosensor made it feasible to detect trace nitrite just by naked eyes. The high surface-to-volume ratio of NPs and the facile modification of AuNPs make them a perfect tool for point of care testing (POCT). A detection process must not only meet the required prescribed limits, but also record the process "from scratch", which is conducive to the study of harmful substance generation, promote the development of foods or other industries, and prevent the generation of carcinogens. In summary, a new nitrite detection nanosensor was developed that has important applications in food detection and cancer prevention. The combination of the surface modified NPs and the traditional chemical reaction could be a very promising research area.

Conflicts of interest

There are no conflicts to declare.

Acknowledgements

This work was supported by the National Key R&D Program of China [grant number: 2016YFD0400800]; National Natural Science Foundation of China (grant numbers: 51763019, U1832125).

References

1 R. Siegel, D. Naishadham and A. Jemal, *Ca-Cancer J. Clin.*, 2013, **63**, 11–30.
2 Z. Fredj, S. Azzouzi, A. P. F. Turner, M. B. Ali and W. C. Mak, *Sens. Actuators, B*, 2017, **248**, 77–84.
3 C. P. Turner and W. R. Carlile, *Acta Hortic.*, 1982, **126**, 213–218.
4 R. Zhong, Y. Liu, P. Zhang, J. Liu, G. Zhao and F. Zhang, *ACS Appl. Mater. Interfaces*, 2014, **6**, 19465–19470.
5 Y. Liu, R. Zhong, P. Zhang, Y. Ma, X. Yun, P. Gong, J. Wei, X. Zhao and F. Zhang, *ACS Appl. Mater. Interfaces*, 2016, **8**, 2478–2485.
6 H. Ohnishi, S. Iwanaga, K. Kawazoe, K. Ishizawa, S. Orino, S. Tomita, K. Tsuchiya, Y. Kanematsu, N. Harada and K. Mori, *J. Agric. Food Chem.*, 2008, **56**, 10092–10098.
7 D. Kumar, B. G. Branch, C. B. Pattillo, *et al.*, *Proc. Natl. Acad. Sci. U. S. A.*, 2008, **105**, 7540–7545.
8 P. Knekt, R. Jãrvinen, J. Dich and T. Hakulinen, *Int. J. Cancer*, 2015, **80**, 852–856.
9 Y. Ma, Y. Wang, D. Xie, *et al.*, *ACS Appl. Mater. Interfaces*, 2018, **10**, 6541–6549.
10 G. M. Hare, A. Mu, A. Romaschin, A. K. Tsui, N. Shehata, W. S. Beattie and C. D. Mazer, *Can. J. Anaesth.*, 2012, **59**, 348–356.
11 D. E. Schwab, J. S. Stamler and D. J. Singel, *Inorg. Chem.*, 2010, **49**, 6330–6342.
12 J. W. Smith, R. K. Lam, O. Shih, A. M. Rizzuto, D. Prendergast and R. J. Saykally, *J. Chem. Phys.*, 2015, **143**, 159–520.
13 Z. Wang, J. Wang, Z. Xiao, J. Xia, P. Zhang, T. Liu and J. Guan, *Analyst*, 2013, **138**, 7303–7317.
14 J. Huang, P. Liu, Q. Sun, H. Zhang, Y. Zhang and K. Wang, *Anal. Lett.*, 2017, **50**, 1620–1629.
15 D. Tsikas, A. Schwarz and D. O. Stichtenoth, *Anal. Chem.*, 2010, **82**, 2585–2587.
16 D. Tsikas, A. Böhmer and A. Mitschke, *Anal. Chem.*, 2010, **82**, 5384–5390.
17 D. Tsikas, A. Mitschke, F. M. Gutzki, S. Engeli and J. Jordan, *Anal. Biochem.*, 2010, **397**, 126–128.
18 K. Ito, R. Nomura, T. Fujii, M. Tanaka, T. Tsumura, H. Shibata and T. Hirokawa, *Anal. Bioanal. Chem.*, 2012, **404**, 2513–2517.
19 D. Tsikas, M. T. Suchy, A. Mitschke, B. Beckmann and F. M. Gutzki, *Methods Mol. Biol.*, 2012, **844**, 277–293.
20 D. Yu, D. Yong and S. Dong, *J. Environ. Sci. (English)*, 2013, **25**, 785–790.
21 Z. Feng, *J. Chin. Inst. Food Sci. Technol.*, 2011, **11**, 192–196.
22 S. Radhakrishnan, K. Krishnamoorthy, C. Sekar, J. Wilson and J. K. Sang, *Appl. Catal., B*, 2014, **148–149**, 22–28.

23 P. Miao, M. Shen, L. Ning, G. Chen and Y. Yin, *Anal. Bioanal. Chem.*, 2011, **399**, 2407–2411.
24 S. Sakthinathan, S. Kubendhira, S. M. Chen, F. M. A. Al-Hemaid, W. C. Liao, P. Tamizhdurai, S. Sivasanker, M. A. Alic and A. A. Hatamleh, *RSC Adv.*, 2016, **6**, 107416–107425.
25 P. Tamizhdurai, S. Sakthinathan, Sh. M. Chen, K. Shanthi, S. Sivasanker and P. Sangeetha, *Sci. Rep.*, 2017, **7**, 46372.
26 L. D. Weston, S. H. Min, L. Jae-Seung and A. M. Chad, *J. Am. Chem. Soc.*, 2009, **131**, 6362–6363.
27 L. Zhao and Y. Hongtao, *Acta Chim. Sin.*, 2012, **70**, 1104–1108.
28 A. Üzer, Z. Can, I. Akın, E. Erçağ and R. Apak, *Anal. Chem.*, 2014, **86**(1), 351–356.
29 M. Stobiecka, *Biosens. Bioelectron.*, 2014, **55**, 379–385.
30 J. Yang, D. Shen, L. Zhou, W. Li, J. Fan, A. M. Eltoni, W. X. Zhang, F. Zhang and D. Zhao, *Adv. Healthcare Mater.*, 2014, **3**, 1620–1628.
31 P. Gobbo, M. C. Biesinger and M. S. Workentin, *Chem. Commun.*, 2013, **49**, 2831–2840.
32 H. X. Su, Z. H. Zhang, X. Y. Zhao, Z. Li, F. Yan and H. Zhang, *Spectrosc. Spectral Anal.*, 2013, **33**, 3180–3187.
33 P. Bajt, *Lambert-Beer's law*, 2018.
34 Z. Zhang, Z. Chen, D. Pan and L. Chen, *Langmuir*, 2015, **31**, 643–650.
35 M. R. Hauwiller, J. C. Ondry, C. M. Chan, P. Khandekar, J. Yu and A. P. Alivisatos, *J. Am. Chem. Soc.*, 2019, **141**(10), 4428–4437.